Photoactivation experiment on ^{197}Au and its implications for the dipole strength in heavy nuclei

C. Nair,[1] M. Erhard,[1] A. R. Junghans,[1] D. Bemmerer,[1] R. Beyer,[1] E. Grosse,[1,2] J. Klug,[1,*] K. Kosev,[1] G. Rusev,[1,†] K. D. Schilling,[1] R. Schwengner,[1] and A. Wagner[1]

[1]*Institut für Strahlenphysik, Forschungszentrum Dresden-Rossendorf, D-01314 Dresden, Germany*

[2]*Institut für Kern- und Teilchenphysik, Technische Universität Dresden, D-01062 Dresden, Germany*

(Received 15 August 2008; published 26 November 2008)

The ^{197}Au(γ, n) reaction is used as an activation standard for photodisintegration studies on astrophysically relevant nuclei. At the bremsstrahlung facility of the superconducting electron accelerator ELBE (Electron Linear accelerator of high Brilliance and low Emittance) of Forschungszentrum Dresden-Rossendorf, photoactivation measurements on ^{197}Au have been performed with bremsstrahlung endpoint energies from 8.0 to 15.5 MeV. The measured activation yield is compared with previous experiments as well as with calculations using Hauser-Feshbach statistical models. It is shown that the experimental data are best described by a two-Lorentzian parametrization with taking the axial deformation of ^{197}Au into account. The experimental ^{197}Au(γ, n) reaction yield measured at ELBE via the photoactivation method is found to be consistent with previous experimental data using photon scattering or neutron detection methods.

DOI: 10.1103/PhysRevC.78.055802 PACS number(s): 25.20.Dc, 26.30.−k, 27.80.+w

I. INTRODUCTION

Photonuclear processes are among the first nuclear reactions ever studied in the laboratory [1]. They have provided important information about the giant dipole resonance (GDR) [2] and play a vital role in our understanding of the cosmic nucleosynthesis pointed out by Burbidge *et al.* [3]. In high temperature cosmic scenarios like exploding supernovas, the photon flux is intense enough to cause the photodisintegration of previously formed heavy nuclides. The photonuclear cross sections are of importance for the understanding of neutron capture in hot and neutron-rich stellar environments, where nuclei are likely to be excited from their ground states and may simultaneously undergo capture. The usual laboratory study of radiative neutron capture does not yield direct information on such processes, but their inverse, photon-induced neutron emission to excited states may reveal respective information via the detailed balance principle [4].

More generally, the combined information from photodisintegration and photon scattering allows us to derive the photon strength function (PSF) below and above the separation energies. The PSF is an essential ingredient for the modeling of astrophysical reaction rates for network calculations of the cosmic nucleosynthesis. The other component of such investigations is the Hauser-Feshbach statistical model (HFM). Accurate experimental studies of the excitation functions of photon-induced processes allow sensitive tests of the parameters entering the model calculations, e.g., optical-model potentials, level densities, and transmission coefficients.

From photoneutron studies concentrating on the GDR region, the accuracy needed for a detailed prediction of the yields of heavy nuclei produced by neutron capture via s and r processes cannot be reached [5]. For the neutron-deficient p nuclei, there is practically no experimental data existing in the astrophysically relevant energy region [6]. In view of the emerging novel observations of isotopic yields in stellar plasma and in gathered cosmic material, high accuracy network calculations are of increasing interest.

The photoneutron cross section of ^{197}Au has been measured by various methods. It has been shown that the cross sections in the isovector GDR region as measured at different laboratories may differ beyond their statistical and systematic uncertainties [2]. Recently, the photoneutron cross section of ^{197}Au has been measured with laser-induced Compton backscattered (LC) photons at the TERAS storage ring at AIST Tsukuba, Japan [7]. Photoactivation of Au has also been investigated recently with bremsstrahlung at an extremely stable clinical accelerator [8].

The ^{197}Au(γ, n) reaction is used as an activation standard for photodisintegration studies on astrophysically relevant nuclei. In this article we present a study of the ^{197}Au(γ, n) reaction for the whole region from the neutron threshold S_n to beyond the top of the GDR with an accuracy of nearly 10%. The bremsstrahlung endpoint energies for the measurements range from 8.0 to 15.5 MeV. Special care was taken at each accelerator setting to measure the bremsstrahlung endpoint energy without relying on the magnetic beam transport elements. The photon flux was determined by an independent observation of photon scattering from ^{11}B exposed to the same photons as the Au samples. The residual nucleus ^{196}Au produced from the ^{197}Au(γ, n) reaction was studied by γ-ray spectroscopy.

Sections II and III describe the experimental procedure and the data analysis. In Sec. IV A, the experimental activation yield is compared to the yield calculated using cross sections from previous experiments on ^{197}Au(γ, n).

In Sec. IV B, the experimental yield is compared with Hauser-Feshbach model calculations. It is shown that the predictions of these models deviate from the measured activation yield.

---

[*]Present address: Ringhals Nuclear Power Plant, SE-43022 Väröbacka, Sweden.

[†]Present address: Department of Physics, Duke University, Triangle Universities Nuclear Laboratory, Durham, NC 27708, USA.

A phenomenological parametrization of the photon strength function is proposed that describes the experimental data and extrapolates it well to the threshold region. Section IV C of this article is devoted to the description of this parametrization and to its comparison with data from photoneutron and photon-scattering studies as well as the comparison with other descriptions of the photon strength function.

II. EXPERIMENTAL SETUP

The experiments were performed at the superconducting electron accelerator ELBE (Electron Linear accelerator of high Brilliance and low Emittance) of the Forschungszentrum Dresden-Rossendorf. ELBE can produce intense bremsstrahlung beams with endpoint energies from 6 to 18 MeV. With these beam parameters both photon scattering and photodisintegration reactions have been measured [9–13].

The bremsstrahlung facility is shown in Fig. 1. The electron beam is focused onto a niobium radiator with thicknesses varying between 1.7 and 10 mg/cm^2 (corresponding to $1.6 \cdot 10^{-4}$ and $1 \cdot 10^{-3}$ radiation lengths) that creates typical "thin target" bremsstrahlung. After passing the radiator, the electrons are deflected by a dipole magnet and dumped to a graphite cylinder mounted on insulating rods surrounded by a water cooled vacuum vessel (electron beam dump, see Fig. 1). A collimator placed 1 m behind the radiator is used to form a beam with a defined diameter out of the spatial distribution of photons. The collimator is made from high-purity aluminum and is fixed within the 1.6 m thick wall of heavy concrete between the accelerator hall and the experimental cave. An aluminum cylinder 10 cm in diameter and 10 cm in length placed in a vacuum chamber in front of the entrance of the collimator acts as a hardener that absorbs mainly low energy photons and thus "hardens" the photon spectrum.

At the target site, the bremsstrahlung beam is collimated onto the ^{197}Au targets sandwiched with a ^{11}B sample. The photon flux is determined experimentally by means of the known integrated cross sections of the states in ^{11}B depopulating via γ rays. Photons scattered from ^{11}B are measured with four high-purity germanium (HPGe) detectors of 100% relative efficiency that are surrounded by escape-suppression shields consisting of bismuth-germanate (BGO) scintillation detectors. The experimental procedure has been described in detail elsewhere [14,15].

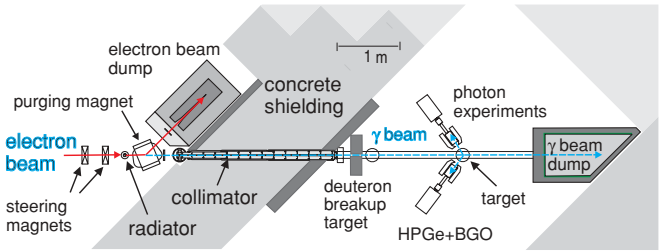

FIG. 1. (Color online) The bremsstrahlung facility at ELBE. The Au targets were irradiated together with ^{11}B samples at the target site. The photons scattered from ^{11}B samples were measured using four 100% HPGe detectors with BGO escape-suppression shields, two of which were mounted vertically (not shown). The endpoint energy of the bremsstrahlung was determined from the proton spectrum of the deuteron breakup reaction.

The ^{197}Au targets used were thin discs with a typical mass of about 200 mg, a thickness of 0.02 mm, and a diameter of 20 mm. The number of activated nuclei produced during the activation was determined offline by measuring the decay of daughter nuclei in a low-level counting setup by HPGe detectors with relative efficiencies of 90 or 60%.

The endpoint energy of the bremsstrahlung distribution is determined by measuring protons from the photodisintegration of the deuteron (see Fig. 1, deuteron breakup target) with silicon detectors. From the maximum energy of the emitted protons, the maximum energy of the incident photons can be deduced. This is described in detail in Sec. III C. During the experiment, energy drifts of the electron linac have been kept to below 1% using nondestructive beam-diagnostics of the transverse beam dispersion and an active beam-stabilization control loop.

III. DATA ANALYSIS

The data deduction and analysis methods are described in detail in the following sections. The discussion is split into three parts:

(i) decays observable following the ^{197}Au(γ, n) reaction and determination of the photoactivation yield;
(ii) experimental determination of the photon flux at the scattering site, and
(iii) bremsstrahlung endpoint energy determination using the deuteron breakup reaction.

A. ^{196}Au decay

The ^{197}Au(γ, n) reaction produces the unstable nucleus ^{196}Au that decays either to ^{196}Pt by electron capture or positron emission (EC + β^+) or to ^{196}Hg by β decay (β^-). A typical decay spectrum of a ^{197}Au sample irradiated with a bremsstrahlung endpoint energy of 14.5 MeV for 17 h is given in Fig. 2. The prominent peaks in the decay of ^{196}Au used for analysis are marked in Fig. 2 and are given in Table I. The decay properties given in the table are adopted from Ref. [16].

TABLE I. Decay properties of the ^{196}Au nucleus.

Nuclide[a]	E_γ (keV)[b]	p[c]
^{196}Pt	333.03(5)	0.229(10)
^{196}Pt	355.73(5)	0.87(3)
^{196}Hg	426.10(8)	0.066(3)

[a]Daughter nuclide from ^{196}Au decay.
[b]Energy of the transition with absolute uncertainty given in parentheses.
[c]Photon emission probability per decay with absolute uncertainty given in parentheses.

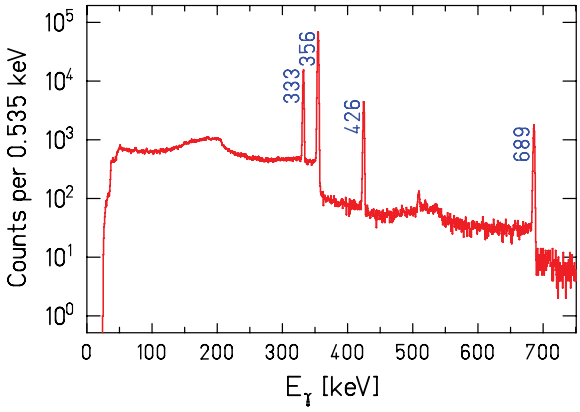

FIG. 2. (Color online) Spectrum of an irradiated ^{197}Au target. The target was placed on the top of a HPGe detector with 90% relative efficiency. The peaks originating from the ^{196}Au decay are marked. The γ line at 689 keV is the sum of the γ transitions with energies 333 and 356 keV. A 1.5 mm thick Cd absorber was used to suppress coincidence summing and low energy x rays.

The absolute photopeak efficiency of the counting setup was determined with several calibration sources from PTB and Amersham (systematic uncertainty in activity 0.6–1.5%) in the energy range from 0.12 to 1.9 MeV.[1] The absolute efficiency was simulated for a realistic geometry using the Monte Carlo code GEANT3 [17] and was fitted to the measured data. Coincidence summing effects depend strongly on the decay scheme. They were determined very precisely for the corresponding counting geometry. The distance between the surface of the endcap and detector crystal was cross-checked by x-ray radiography. The number of γ rays counted in the peaks at 333 and 356 keV were corrected for "summing-out" events using the method described in Ref. [18]. For the transition at 333 keV, the coincidence summing correction amounts to 24% and for 356 keV it is 6%, both with a relative uncertainty of 5%.

In a photoactivation experiment, the number of radioactive nuclei $N_{\mathrm{act}}(E_0)$ produced is proportional to the integral of the absolute photon fluence $\Phi_\gamma(E, E_0)$ times the photodisintegration cross section $\sigma_{\gamma,\mathrm{n}}(E)$ integrated from the reaction threshold energy E_{thr} up to the endpoint energy E_0 of the bremsstrahlung spectrum.

$$N_{\mathrm{act}}(E_0) = N_{\mathrm{tar}} \cdot \int_{E_{\mathrm{thr}}}^{E_0} \sigma_{\gamma,n}(E) \cdot \Phi_\gamma(E, E_0)\, dE. \qquad (1)$$

The number of radioactive nuclei $N_{\mathrm{act}}(E_0)$ is determined experimentally by measuring the activity of the irradiated sample using

$$N_{\mathrm{act}}(E_0) = \frac{N_\gamma(E_\gamma, E_0) \cdot \kappa_{\mathrm{corr}}}{\varepsilon(E_\gamma) \cdot p(E_\gamma)}. \qquad (2)$$

$N_\gamma(E_\gamma, E_0)$, $\varepsilon(E_\gamma)$, and $p(E_\gamma)$ denote the dead-time and pile-up corrected full-energy peak counts of the observed transition, the absolute efficiency of the detector at the energy E_γ, and the emission probability of the photon with energy E_γ, respectively.

The factor κ_{corr} in Eq. (2) is given by

$$\kappa_{\mathrm{corr}} = \frac{\exp\left(\frac{t_{\mathrm{loss}}}{\tau}\right)}{1 - \exp\left(\frac{-t_{\mathrm{meas}}}{\tau}\right)} \cdot \frac{\frac{t_{\mathrm{irr}}}{\tau}}{1 - \exp\left(\frac{-t_{\mathrm{irr}}}{\tau}\right)}. \qquad (3)$$

This expression determines the number of radioactive nuclei from their decays measured during the time t_{meas}. It also takes into account decay losses during irradiation (t_{irr}) and in between the end of the irradiation and the beginning of the measurement (t_{loss}). The mean lifetime of the radioactive nucleus produced during the photoactivation is denoted by τ. The decay time constants of ^{196}Au and ^{198}Au have been confirmed in a precision measurement using targets produced in the scope of the present experiment [19].

The activation yield is denoted by Y_{act} and is expressed as the ratio of the number of activated nuclei to the number of target atoms in the sample. For the ^{197}Au(γ, n) reaction,

$$Y_{\mathrm{act}} = \frac{N_{\mathrm{act}}(^{196}\mathrm{Au})}{N_{\mathrm{tar}}(^{197}\mathrm{Au})}. \qquad (4)$$

Using Eq. (1), the activation yield can be calculated from $\sigma_{\gamma,n}(E)$ data with the known bremsstrahlung spectrum. In this way measured activation yields can be compared with the experimental or theoretical cross section data.

B. The photon flux

In the present study, the photon flux was determined from the elastic photon scattering from a ^{11}B sample sandwiched with the Au activation target. Four HPGe detectors (two at 90° and two at 127°) were used for this measurement (see Ref. [14] for details). The photon fluence is determined experimentally using the formula

$$\Phi_\gamma(E_\gamma) = \frac{N_\gamma(E_\gamma)}{\varepsilon(E_\gamma) \cdot N_{\mathrm{tar}} \cdot I_{\mathrm{s}} \cdot \mathrm{W}(\theta)}. \qquad (5)$$

$N_\gamma(E_\gamma)$, $\varepsilon(E_\gamma)$, and N_{tar} represent the dead-time and pile-up corrected full-energy peak counts of the resonant transition, the absolute efficiency of the detector at the energy E_γ, and the number of target atoms in the ^{11}B sample. $W(\theta)$ is the angular correlation between the incoming and scattered photon and I_{s} denotes the integrated scattering cross section.

The decay properties of calibration transitions were adopted from the online library of Evaluated Nuclear Structure Data Files (ENSDF), which refers to the revised Ajzenberg-Selove compilation (see Table 11.4, Ref. [20]). The absolute photopeak efficiency has been determined with calibration sources for energies up to 1.9 MeV. For extrapolating the efficiency to higher energies, a GEANT3 simulation under realistic geometry was used (see Fig. 4, Ref. [13]). The simulations were normalized to the measured efficiency at energies below 1.9 MeV.

In a typical case, the ^{11}B target used was of metallic boron powder with an enrichment of 99.5%, a mass areal density of 1.43 g cm^{-2}, and an effective density of 1.6 g cm^{-3}. Energy dependent nuclear self-absorption corrections were

[1]PTB: Physikalisch-Technische Bundesanstalt, Fachbereich 6.1, Bundesallee 100, Braunschweig, Germany; Amersham: ISOTRAK AEA Technology QSA, Gieselweg 1, Braunschweig, Germany.

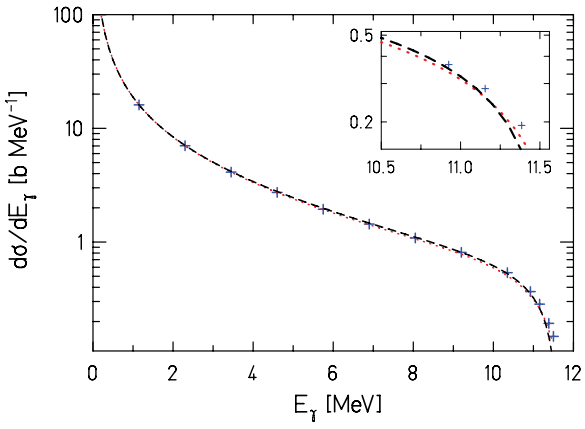

FIG. 3. (Color online) Comparison of theoretical bremsstrahlung cross sections for the Nb radiator for an incident electron endpoint energy of 11.5 MeV. Dashed and dotted lines correspond to the bremsstrahlung distributions by Schiff [22] and Haug [23], whereas values created from the Seltzer and Berger [24] tables are shown as symbols (+).

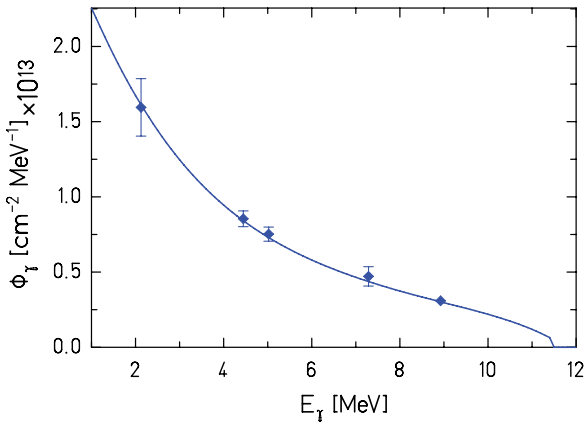

FIG. 4. (Color online) Absolute photon fluence measured from the scattered photons in ^{11}B is compared with the Seltzer and Berger [24] bremsstrahlung spectra with hardener corrections. The fluence measured with different transitions in ^{11}B agree with the simulated curve to within 6%.

applied using the formalism given in Ref. [21]. For example, for the transition at 7.288 MeV, the nuclear self-absorption correction amounts to about 7.5% when using a target with the specifications given above.

The bremsstrahlung spectrum is well approximated by the theoretical bremsstrahlung distribution for a thin niobium target. Different approaches are compared for the niobium radiator for an incident electron endpoint energy of 11.5 MeV as shown in Fig. 3. They agree well with recent quantum mechanical calculations by Haug [23] and Roche, Ducos, and Proriol [25], which use the atomic shielding effects given in Ref. [26].

At the low energy side of the spectrum the different theoretical approaches are not distinguishable from each other and agree within 1%. Near endpoint, the theoretical models differ by about 20% (see inset, Fig. 3). The theoretical description of the high energy end of the bremsstrahlung distribution has a systematic effect on the calculation of the activation yield from a given photoneutron cross section (see Sec. IV A). For an endpoint energy of 9 MeV or higher, the ^{197}Au(γ, n) activation yield calculated with the cross section from Haug [23] would be 5% lower than that calculated with the cross section from Seltzer and Berger [24]. Below 9 MeV this effect increases up to 30%.

The experimental photon fluences determined from the ^{11}B(γ, γ') reaction for the γ transitions at 2.125, 4.446, 5.022, 7.288, and 8.924 MeV are shown in Fig. 4. The bremsstrahlung spectrum was simulated using MCNP [27] to take into account the effects of the aluminum hardener situated behind the niobium radiator. In MCNP, the bremsstrahlung cross sections from Seltzer and Berger [24] are used. The simulated bremsstrahlung spectrum has been normalized to the measured absolute photon fluence at the transition energies of ^{11}B. The systematic deviations between the simulated curve and the experimental points are about 6%.

In the fluence determination procedure discussed above, the statistical contribution to the uncertainties from the γ counting is quite small and is of the order of 0.5–2%. The systematic uncertainty in the extrapolation of efficiency is estimated to be about 5% in the energy range of the observed transitions in ^{11}B.

C. Determination of bremsstrahlung endpoint energy

For the experiments described here, it is necessary to measure the endpoint energy of the bremsstrahlung spectra precisely. An online measurement of the beam energy is attained using the dispersion inside a dipole magnet with a magnetic field integral $\int B\mathrm{d}l$ known to about 1% only [28]. Therefore, we employed a different method for the beam energy determination that is based on the spectroscopy of protons in the photodisintegration of the deuteron—the ^{2}H$(\gamma, p)n$ reaction. From the pure two-body kinematics, the energy of the incident photon can be deduced directly from the measured energy of the emitted proton.

The protons from the photodisintegration of the deuteron are detected by a setup of four silicon detectors (Ion-Implanted-Silicon Charged-Particle Detectors, type ORTEC ULTRA)[2] placed at a distance of 115 mm from the beam axis and at azimuthal angles of 0°, 90°, 180°, and 270° with respect to the photon beam. The detectors have a thickness of 500 μm and a sensitive area of 600 mm^2. A 4 mg/cm^2 thick polyethylene film, in which hydrogen is substituted by deuterium (CD_2)[3] is used as a target. The CD_2 target is positioned parallel to the incident beam such that its surface is observed by all four detectors under 45°. A typical spectrum is shown in Fig. 5. The low-energy part of the spectrum below 2.5 MeV is not useful as it is dominated by beam-induced background.

To determine the endpoint energy, a simulated spectrum is fitted to the measured proton spectrum. The simulation takes into account the deuteron breakup kinematics, the geometry of

[2]ORTEC, 801 South Illinois Avenue, Oak Ridge, TN 37830, USA.
[3]Courtesy of D. K. Geiger, SUNY Geneseo, NY 14454, USA.

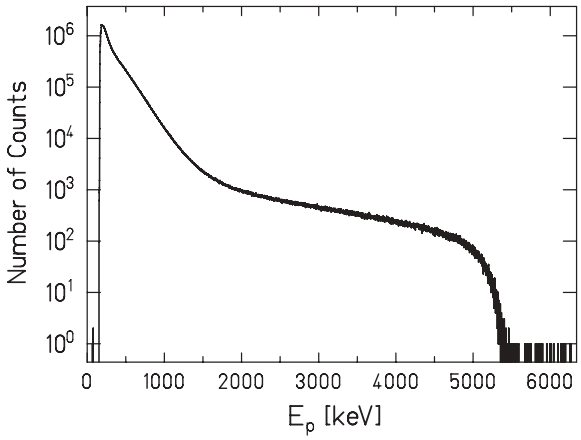

FIG. 5. Proton spectrum from the photodisintegration of deuterons, recorded with Si detectors of 500 μm thickness during an irradiation with incident electron energy 13.2 MeV.

the detector setup, the energy loss of the protons inside the CD_2 film, and the energy spread of the electron beam. The fit to the measured spectra is shown in Fig. 6. The statistical error from the fit amounts to 2–8 keV for the range of energies described here. The systematic deviation of the experimental spectra to the simulated one is 40 keV. This is inherent to all experiments but significant only for endpoint energies close above the neutron emission threshold of the ^{197}Au(γ, n) reaction.

IV. RESULTS AND DISCUSSION

Photoactivation experiments with bremsstrahlung have the limitation that the data need to be unfolded to obtain a cross section [29]. This requires precise knowledge of the bremsstrahlung spectrum especially close to the endpoint and data with very high counting statistics on a fine grid of endpoint energies. In this work, the measured photoactivation yield is presented and compared to calculated yield curves.

For the ^{197}Au(γ, n) reaction, the photoactivation yield is determined as described by Eq. (4). The activation yield is normalized to the photon fluence for the corresponding

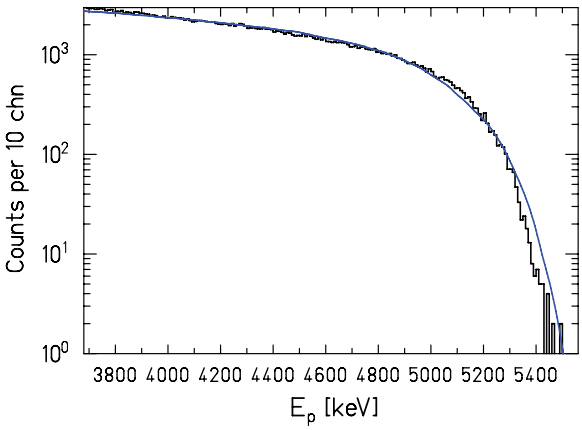

FIG. 6. (Color online) The simulated proton spectrum (line) is fitted to the measured spectrum (histogram) from Fig. 5.

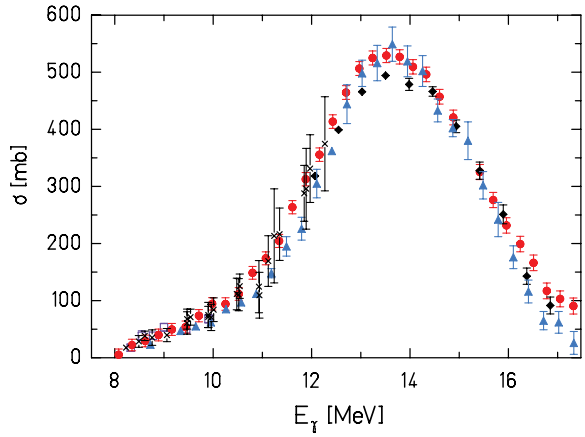

FIG. 7. (Color online) Photoneutron cross sections for ^{197}Au(γ, n) from previous experiments. The symbols denote data from the respective experiments: triangles, Fultz *et al.* [30]; diamonds, Berman *et al.* [31]; and circles, Veyssiere *et al.* [32]. Some ^{197}Au(γ, n) cross section data below 10 MeV have been derived from bremsstrahlung activation by Vogt *et al.* (open squares) [33]. Also shown are cross sections determined from Laser-Compton scattering by Hara *et al.* (×) [7].

measurement as discussed in Sec. III B. The endpoint energies were determined from the photodisintegration of the deuteron as explained in Sect. III C. The experimental activation yield normalized to the photon fluence is compared with previous experimental data as well as with model calculations.

A. Activation yield: Comparison with previous experiments

In this section, the activation yield from the ELBE experiments is compared with calculated yields using cross sections measured in previous experiments. A comparison of the ^{197}Au(γ, n) cross sections from previous experiments [30–33] is given in Fig. 7. At the Lawrence Livermore National Laboratory (LLNL), the photoneutron cross section of the nucleus ^{197}Au has been measured with quasi-monoenergetic photons from the positron annihilation technique. There are two sets of published data—first by Fultz *et al.* [30] and later by Berman *et al.* [31]. The same technique has been used by Veyssiere *et al.* [32] at Saclay (France) for studying photoneutron reactions on ^{197}Au. The results from Livermore and Saclay are not in agreement, revealing the differences in the neutron multiplicity determination procedure used in both laboratories.

Berman *et al.* [31] have remeasured photoneutron cross sections with quasi-monoenergetic photons at LLNL, with special emphasis on determining the absolute cross section at energies across the peak of the GDR. Based on this experiment, Berman *et al.* [31] resolves the differences by recommending a 7% scaling on the Veyssiere data [32] and ignoring the Fultz data [30] (see Table VI, Ref. [31]). We adopt this recommendation for comparing the ELBE data with the previously reported values.

At the Laser-Compton scattering facility at the TERAS storage ring at AIST Tsukuba, quasi-monoenergetic photons were used to study photoneutrons from ^{197}Au(γ, n) up to

12.4 MeV. These data agree very well with the data measured with the positron anihilation technique but because a photon difference method was used they have a rather large experimental uncertainty.

The photoneutron cross section of ^{197}Au for energies close above the (γ, n) threshold has been deduced by Vogt *et al.* [33] using photoactivation with bremsstrahlung at the S-DALINAC (Darmstadt). The cross sections are in agreement with the data of Veyssiere *et al.* [32], but exist only for endpoint energies between 8.0 and 10.0 MeV.

The total nuclear photoabsorption cross section of ^{197}Au was measured at the synchrotron facility of the Institute of Nuclear Research (Moscow) by Gurevich *et al.* [34]. Even though the data agree with the measurements by Veyssiere *et al.* [32], they exhibit significant scatter (Fig. 2, Ref. [34]). The tabulated errors are quite big and therefore were not included for comparison with the ELBE data reported here. The photoneutron yield for ^{197}Au was measured by Sorokin, Krushchev, and Yurev [35] at the Betatron (Moscow State University) and the cross sections were deduced by the Penfold-Leiss [36] method. This experiment was done with an energy resolution of 0.5 MeV for the range of energies considered here. The results from Sorokin *et al.* [35] are not included in the present discussion because the uncertainties resulting from the unfolding process are very large and the data differ significantly from the previous experimental data.

In Fig. 8, the experimental activation yield from ELBE is compared to the yield calculated using the cross sections measured previously. The activation yield is normalized to the photon fluence measured from the scattered photons in ^{11}B (see Sec. III B). The experimental yield from ELBE is in agreement with the yield calculated using the cross sections from Vogt *et al.* [33] for the close-threshold endpoint energies up to 10 MeV. The activation yield calculated using cross sections from Veyssiere *et al.* [32] is in agreement with the ELBE yield for the whole range of energies. Close to the neutron emission threshold, the reaction yield strongly depends on the endpoint energy E_0 of the bremsstrahlung beam. In this case, small uncertainties in E_0 result in large uncertainties in the activation yield.

The uncertainties in the experimental points shown in Fig. 8 are mainly from the determination of photon fluence as discussed in Sec. III B. The statistical uncertainties are very small and in the order of about 0.5–2%. The major systematic uncertainties arise from the extrapolation of measured photopeak efficiencies to the higher energies in ^{11}B transitions (5%) and in the systematic deviation of measured photon fluence from the simulated curve (6%). The systematic errors have been added quadratically and amount to about 7.8% but are not shown in Fig. 8.

B. Activation yield: Comparison with model calculations

Figure 9 compares the experimental activation yield to the simulated yield calculated using cross sections predicted by Hauser-Feshbach models [37,38]. Simulations using the TALYS [37] and NON-SMOKER [38] codes describe the experimental data only to a factor of 2. Both calculations were performed using cross sections derived from standard input parameters. The default option of TALYS for the GDR parameters originates from the Beijing GDR compilation, as present in the RIPL database [39].

In the case of (γ, n) reactions, one crucial ingredient for the model calculation is the photon strength function. As the (γ, n) channel in ^{197}Au is the dominant decay channel for the energy range above threshold, the photon strength distribution directly determines the calculated (γ, n) cross section and the reaction yield. In the model calculations care is also taken for the fact that the (γ, p) channel is open above 5.8 MeV. Due to the large Z, the p emission is strongly suppressed by the Coulomb

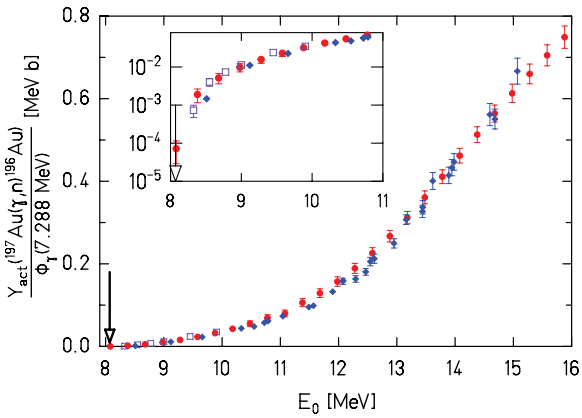

FIG. 8. (Color online) The activation yield for the ^{197}Au(γ, n) reaction normalized to the photon fluence is compared to the yield calculated using cross sections measured in previous experiments. The present data are denoted by diamonds with an arrow pointing to the neutron emission threshold. Reaction yields calculated using the cross sections given by Veyssiere *et al.* [32] (circles) and Vogt *et al.* [33] (open squares) are in good agreement with the yield measured at ELBE.

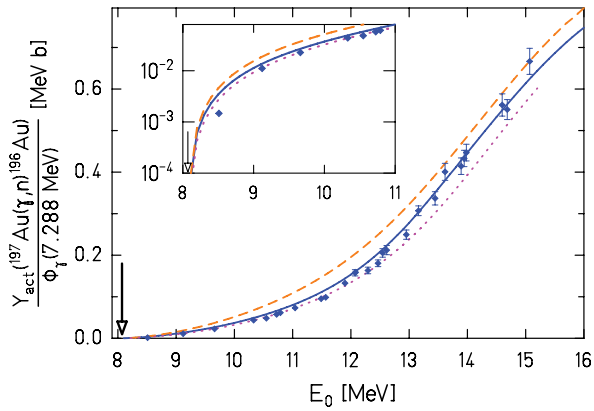

FIG. 9. (Color online) Experimental activation yield normalized to the photon fluence for the ^{197}Au(γ, n) reaction compared to theoretical model calculations. The experimental data are denoted by diamonds with a downward arrow denoting the neutron emission threshold. The dashed and dotted lines denote yield calculations using cross sections from the TALYS [37] and NON-SMOKER [38] codes, respectively. The solid line represents a TALYS calculation with modified inputs, see text.

interaction. With default inputs, the TALYS calculation yields a (γ, p) cross section that is about four orders of magnitude smaller than the (γ, n) cross section.

The activation yields calculated using TALYS with different optical model potentials, like Koning-Delaroche and Jeukenne-Lejeune-Mahaux (JLM), are very similar, demonstrating that the ^{197}Au(γ, n) reaction yield is not sensitive to the choice of optical model parameters. The sensitivity to the photon strength function is larger. We modified the deformation dependent parameters of the $E1$ strength function used in TALYS according to a new phenomenological parametrization. The improved new parametrization explains the experimental data better than the statistical models with default inputs and is discussed in the following section in detail.

C. Phenomenological parametrization of the photon strength function

If one assumes that the dipole strength in a heavy nucleus is dominated by the GDR, then the strength function $f_1(E_\gamma)$ according to Bartholomew *et al.* [40] is related to the average photoabsorption cross section $\langle\sigma_\gamma(E_\gamma)\rangle$ by

$$\frac{\langle\sigma_\gamma(E_\gamma)\rangle}{3(\pi\hbar c)^2 \cdot E_\gamma} = f_1(E_\gamma) = \frac{\langle\Gamma_{E_1}\rangle}{E_\gamma^3 \cdot D}, \tag{6}$$

with $\langle\Gamma_{E_1}\rangle$ and D denoting the average photon width and the average level spacing at the endpoint of electromagnetic transition. A new phenomenological description based on the ground state deformation parameters describes well the average photon absorption for nuclei with $A > 80$ from $E_x \approx 4$ MeV up to several MeV above the GDR [41].

A consistent description holds for the photon strength distribution in spherical, transitional, triaxial, and well-deformed nuclei. In nearly all nuclei the GDR is split into two or three components, whose energies are well predicted by the finite range droplet model (FRDM) [42]. The splitting [43] is due to the three different axes of the ellipsoid parameterizing the nuclear shape with its deformation parameter β and triaxiality parameter γ:

$$E_k = \frac{E_0 \cdot R_0}{R_k} = \frac{E_0}{\exp\left[\sqrt{\frac{5}{4\pi}} \cdot \beta \cdot \cos\left(\gamma - \frac{2}{3}k\pi\right)\right]}. \tag{7}$$

This results from the fact that the vibrational frequency $E_k/\hbar$ along a given axis k is inversely proportional to the corresponding semi-axis length R_k. The nuclear radius is given by $R_0 = 1.16\, A^{1/3}$ fm. The GDR centroid energy E_0 given in Ref. [42] of a spherical nucleus with mass A is calculated with an effective nucleon mass $m^* = 874$ MeV/c^2.

The average absorption cross section in the GDR is given by

$$\langle\sigma_\gamma(E_\gamma)\rangle = \frac{1.29 \cdot Z \cdot N}{A} \sum_{k=1}^{3} \frac{E_\gamma^2 \Gamma_k}{\left(E_k^2 - E_\gamma^2\right)^2 + E_\gamma^2 \Gamma_k^2}, \tag{8}$$

where the GDR widths Γ_k to be used in the sum of up to three Lorentzians have been assumed to be constant, in contrast to earlier descriptions [44,45]. The symbols E_γ, E_k denote photon energy and resonance energies given in MeV and $\langle\sigma_\gamma(E_\gamma)\rangle$ given in fm^2. The Thomas-Reiche-Kuhn sum rule as determined from general quantum mechanical arguments [47] is included in this description for the average photon absorption cross section obtained on an absolute scale.

The width Γ_k for the different components of the GDR is dependent on the resonance energy E_k and is generally used for all stable nuclei with $A > 80$,

$$\Gamma_k(E_k) = 1.99 \text{ MeV} \cdot \left(\frac{E_k}{10 \text{ MeV}}\right)^\delta, \tag{9}$$

where $\delta = 1.6$ is taken from the one-body dissipation model [43].

For the case of ^{197}Au we assume that the average of the experimentally determined deformation parameters of the even-mass neighbor nuclei ^{196}Pt and ^{198}Hg [48–50] can be used to describe the shape of the odd nucleus ^{197}Au; we insert $\beta = 0.15$ and $\gamma = 60^\circ$ into Eq. (7). The GDR centroid energy is $E_0 = 13.9$ MeV. These parameters are in accordance with the FRDM and result in the following resonance energies and widths: $E_{1,3} = 13.2$ MeV, $\Gamma_{1,3} = 3.1$ MeV and $E_2 = 15.2$ MeV, $\Gamma_2 = 3.9$ MeV. The TALYS code was modified with these inputs for oblate deformation. The yield curve created using the cross sections resulting from modified inputs is shown in Fig. 9 and is in better agreement with the ELBE data.

The photon strength function of ^{197}Au derived from different theoretical models and compared to experimental data is shown in Fig. 10. The strength function created using the modified inputs as discussed above is compared to the

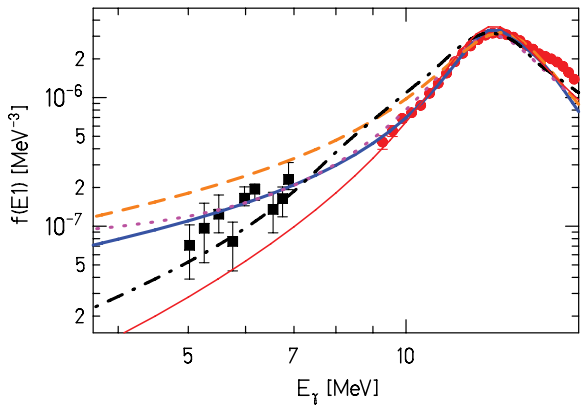

FIG. 10. (Color online) The photon strength function of ^{197}Au derived on the assumption of oblate deformation (solid line) compared to different models. The dashed and dotted lines correspond to the strength functions given by the Brink-Axel [51] and Kopecky-Uhl [44] models, respectively. The microscopic $E1$ photoabsorption strength function determined within the QRPA model [52,53] is shown by the dash-dotted line. All calculations were done using the TALYS code. The Enhanced Generalized LOrentzian (EGLO) model taken from the Reference Input Parameter Library RIPL-2 of the IAEA [39] is shown as a thin solid line. The experimental strength function from Bartholomew *et al.* [40] (squares) below the neutron emission threshold and the strength function derived using the ^{197}Au(γ, n) photoneutron cross section measured by Veyssiere *et al.* [32] (circles) are also shown.

default models [44,51] in TALYS, which treats ^{197}Au as a spherical nucleus. It is clear that the new parameters lead to a reduced strength at energies below the GDR and thus result in a good fit to its shape with a constant spreading width. This agrees well with the experimental strength function given by Bartholomew *et al.* [40] for energies below the neutron emission threshold. Above the separation energy, the strength functions shown were deduced from the ^{197}Au(γ, n) cross sections by Veyssiere *et al.* [32] The strength function derived using the modified parameters gives clearly a better fit to the data than calculations [52,53] on the basis of the quasi-particle random phase approximation (QRPA) with phenomenological correction for deformation.

V. CONCLUSIONS

For the ^{197}Au(γ, n) reaction, the activation yield has been measured and compared with the Hauser-Feshbach model calculations as well as with previous experimental data. The measured activation yield at ELBE is in agreement with the calculated yields using cross sections measured with quasi-monoenergetic photons from positron annihilation in flight and laser-induced Compton backscattering.

The activation experiment discussed here, which was performed in combination with a direct determination of the electron energy via the bremsstrahlung spectrum endpoint, delivers precise photon strength data. Thus they may allow a verification of data obtained previously by direct absorption experiments or by detecting neutrons from the (γ, n) process. They also allow us to make judgements on parametrizations developed for the prediction of the photon strength function as well as on particle transmission functions, i.e., on optical model parameters.

We have demonstrated for the case of ^{197}Au(γ, n) that a sum of two GDR Lorentzians with a small oblate deformation of ^{197}Au determining the energy split and the width difference describes the photon absorption well. The availability of information on the nuclear shape as well as on the PSF below threshold makes ^{197}Au a prime case to perform a consistent test of statistical calculations of Hauser-Feshbach type and to derive a coherent picture of near-threshold processes. The detailed understanding of these has direct importance for the s process as well, because the prediction of the relative abundances of the isotopes of Hg depends on the relative strength of the β decay of ^{198}Au and ^{198}Au(n, γ) in stellar plasmas. Last, but not least, the experimental data reported here for the ^{197}Au(γ, n) reaction may serve as a normalization for future measurements on other nuclei. The ^{197}Au(γ, n) reaction has been used as a photoactivation standard for the experiments discussed in Refs. [54] and [55].

ACKNOWLEDGMENTS

We thank Peter Michel and the ELBE team for providing a stable beam during activation experiments. We are indebted to E. Haug for providing valuable information about the theory of bremsstrahlung and his model codes. Special thanks are due to Rudi Apolle for simulating proton spectra of the deuteron breakup reaction under a realistic geometry. The technical assistance of Andreas Hartmann is gratefully acknowledged. We are grateful to Tom Cowan for a thorough, critical reading of the manuscript.

[1] W. Bothe and W. Gentner, Z. Phys. **106**, 236 (1937); **112**, 45 (1939).
[2] S. S. Dietrich and B. L. Berman, At. Data Nucl. Data Tables **38**, 199 (1988).
[3] E. M. Burbidge, G. R. Burbidge, W. A. Fowler *et al.*, Rev. Mod. Phys. **29**, 547 (1957).
[4] K. Sonnabend, P. Mohr, K. Vogt *et al.*, Astrophys. J. **583**, 506 (2003).
[5] F. Käppeler and A. Mengoni, Nucl. Phys. **A777**, 291 (2006).
[6] M. Arnould and S. Goriely, Phys. Rep. **384**, 1 (2003).
[7] K. Y. Hara, H. Harada, F. Kitatani *et al.*, J. Nucl. Sci. Technol. **44**, 938 (2007).
[8] P. Mohr, S. Brieger, G. Witucki *et al.*, Nucl. Instrum. Methods A **580**, 1201 (2007).
[9] G. Rusev, R. Schwengner, F. Dönau *et al.*, Phys. Rev. C **73**, 044308 (2006).
[10] G. Rusev, E. Grosse, M. Erhard *et al.*, Eur. Phys. J. A **27** s01, 171 (2006).
[11] R. Schwengner, G. Rusev, N. Benouaret *et al.*, Phys. Rev. C **76**, 034321 (2007).
[12] A. Wagner, R. Beyer, M. Erhard *et al.*, J. Phys. G: Nucl. Part. Phys. **35**, 014035 (2008).
[13] G. Rusev, R. Schwengner, F. Dönau *et al.*, Phys. Rev. C **77**, 064321 (2008).
[14] R. Schwengner, R. Beyer, F. Dönau *et al.*, Nucl. Instrum. Methods A **555**, 211 (2005).
[15] A. Wagner, R. Beyer, M. Erhard *et al.*, J. Phys. G: Nucl. Part. Phys. **31**, S1969 (2005).
[16] H. Xiaolong, Nucl. Data Sheets **108**, 1093 (2007).
[17] GEANT3: CERN Program Library Long Writeup Q121, CERN, Geneva (CH), 1994.
[18] K. Debertin and R. G. Helmer, *Gamma- and X-Ray Spectroscopy with Semiconductor Detectors* (Elsevier, Amsterdam/New York, 2001).
[19] G. Ruprecht, C. Vockenhuber, L. Buchmann, R. Woods, C. Ruiz, S. Lapi, and D. Bemmerer, Phys. Rev. C **77**, 065502 (2008).
[20] F. Ajzenberg-Selove, Nucl. Phys. **A506**, 1 (1990).
[21] S. J. Skorka, *Electromagnetic Interaction in Nuclear Spectroscopy*, edited by W. D. Hamilton (North-Holland, Amsterdam, 1975).
[22] L. I. Schiff, Phys. Rev. **83**, 252 (1951).
[23] E. Haug, Radiat. Phys. Chem. **77**, 207 (2008).
[24] S. M. Seltzer and M. J. Berger, At. Data Nucl. Data Tables **35**, 345 (1986).
[25] G. Roche, C. Ducos, and J. Proriol, Phys. Rev. A **5**, 2403 (1972).
[26] F. Salvat, J. D. Martinez, R. Mayol, and J. Parellada, Phys. Rev. A **36**, 467 (1987).
[27] MCNP - Monte Carlo N-Particle Transport Code, http://mcnp-green.lanl.gov/; Version 4C2 obtainable from http://www.nea.fr/abs/html/ccc-0701.html.
[28] M. Justus *et al.*, in Proceedings of DIPAC 2007 - 8th European Workshop on Beam Diagnostics and Instrumentation

for Particle Accelerators, May 20–23, 2007, Venice, Italy; http://www.elettra.trieste.it/dipac07/; http://www.jacow.org/.
[29] B. L. Berman and S. C. Fultz, Rev. Mod. Phys. **47**, 713 (1975).
[30] S. C. Fultz, J. T. Caldwell, R. L. Bramblett *et al*., Phys. Rev. **127**, 1273 (1962).
[31] B. L. Berman, R. E. Pywell, S. S. Dietrich, M. N. Thompson, K. G. McNeill, and J. W. Jury, Phys. Rev. C **36**, 1286 (1987).
[32] A. Veyssiere, H. Beil, R. Bergere *et al*., Nucl. Phys. **A159**, 561 (1970).
[33] K. Vogt, P. Mohr, M. Babilon *et al*., Nucl. Phys. **A707**, 241 (2002).
[34] G. M. Gurevich, L. E. Lazareva, V. M. Mazur *et al*., Nucl. Phys. **A338**, 97 (1980).
[35] Y. I. Sorokin, V. A. Khrushchev, and B. A. Yurev, Izv. Akad. Nauk. SSSR, Ser. Fiz. **33**, 1891 (1973).
[36] A. S. Penfold and J. E. Leiss, Phys. Rev. **114**, 1332 (1959).
[37] A. J. Koning, S. Hilaire, and M. C. Duijvestijn, in *Proceedings of the International Conference on Nuclear Data for Science and Technology - ND2004, Santa Fe, New Mexico, USA, September 26–October 1, 2004*, edited by R. C. Haight, M. B. Chadwick, T. Kawano, and P. Talou, AIP Conf. Proc. **769**, 1154 (2005); http://www.talys.eu.
[38] T. Rauscher and F. K. Thielemann, At. Data Nucl. Data Tables **88**, 1 (2004).
[39] http://www-nds.iaea.org/ripl-2/; http://www-nds.iaea.or.at/reports/indc-ccp-440.pdf.
[40] G. A. Bartholomew, E. D. Earle, A. J. Ferguson *et al*., Adv. Nucl. Phys. **7**, 229 (Plenum Press, New York, 1973).
[41] A. R. Junghans, G. Rusev, R. Schwengner *et al*., Phys. Lett. B (2008) doi: 10.1016/j.physletb.2008.10.055.
[42] W. D. Myers, W. J. Swiatecki, T. Kodama *et al*., Phys. Rev. C **15**, 2032 (1977); P. Möller, J. R. Nix, W. D. Myers *et al*., At. Data Nucl. Data Tables **59**, 185 (1995).
[43] B. Bush and Y. Alhassid, Nucl. Phys. **A531**, 27 (1991).
[44] J. Kopecky and M. Uhl Phys. Rev. C **41**, 1941 (1990).
[45] L. Zanini, F. Corvi, H. Postma F. Becvar, M. Krticka, J. Honzatko, and I. Tomandl, Phys. Rev. C **68**, 014320 (2003).
[46] C. B. Dover *et al*., Ann. Phys. **70**, 458 (1972).
[47] J. M. Eisenberg and W. Greiner, *Nuclear Theory*, Vol. 2, *Excitation Mechanisms of the Nucleus,* 3rd edition (North-Holland, Amsterdam, 1988).
[48] A. Mauthofer, K. Stelzer, J. Idzko *et al*., Z. Phys. A **336**, 263 (1990).
[49] A. Bockisch, A. Bharuth-Ram, A. M. Kleinfeld *et al*., Z. Phys. A **291**, 245 (1979).
[50] N. J. Stone, At. Data Nucl. Data Tables **90**, 75 (2005).
[51] D. M. Brink, Nucl. Phys. **4**, 215 (1957); P. Axel, Phys. Rev. **126**, 671 (1962).
[52] S. Goriely and E. Khan, Nucl. Phys. **A706**, 217 (2002).
[53] E. Khan, T. Suomijarvi, Y. Blumenfeld *et al*., Nucl. Phys. **A694**, 103 (2001).
[54] C. Nair, A. R. Junghans, M. Erhard *et al*., J. Phys. G: Nucl. Part. Phys. **35**, 014036 (2008).
[55] M. Erhard, A. R. Junghans, R. Beyer *et al*., Eur. Phys. J. A **27** s01, 135 (2006).